Applied and Computational Mathematics
2026, Vol. 15, No. 6, pp. 233–243
https://doi.org/10.11648/j.acm.20261506.12

Research Article

A Radial Basis Function Collocation Method for Time-Dependent Partial Differential Equations: Stability, Accuracy, and Recent Advances

Fatemeh Sharafi *

Department of Mathematics, Islamic Azad University, Kerman, Iran

Abstract

This paper presents an advanced analysis of the radial basis function (RBF) collocation method for solving time-dependent partial differential equations (PDEs). A unified framework is developed that integrates weighted finite difference temporal discretization with global RBF spatial approximation for both smooth and piecewise smooth radial kernels. We provide a rigorous stability analysis of the resulting time-stepping scheme and systematically examine the roles of the shape parameter, polynomial augmentation, and scattered point distribution in controlling accuracy and conditioning. In addition to the classical global collocation formulation, we survey and compare contemporary localized and high-order RBF variants—including localized RBF collocation (LRBF), RBF partition of unity (RBF-PU), ghost-point-enhanced RBF pseudo-spectral (RBF-PS-G), and RBF finite difference (RBF-FD)—that have emerged as the state of the art for large-scale and long-time simulations in 2024–2026. Numerical experiments on benchmark problems including the telegraph and Klein–Gordon equations, a nonlinear viscous Burgers equation, a three-dimensional Helmholtz problem, and comparisons between global RBF, RBF-PU, and LRBF validate the theoretical predictions. The method's simplicity, mesh-free nature, and high-order accuracy make it a competitive and highly adaptable tool for a broad class of PDE problems.

Keywords

Meshless Methods, Radial Basis Functions, Collocation Method, Partial Differential Equations, Stability Analysis, Shape Parameter

1. Introduction

Partial differential equations (PDEs) are the mathematical foundation for modeling diverse phenomena in physics, engineering, biology, and finance. Traditional mesh-based methods—finite difference (FD), finite element (FE), and finite volume (FV) methods—rely on a computational mesh that must conform to the problem geometry. For problems with complex or evolving boundaries, mesh generation and maintenance become prohibitively expensive. Meshless methods overcome these difficulties by working directly with scattered node sets, eliminating connectivity information.

Among meshless techniques, radial basis function (RBF) methods occupy a central position due to their simplicity, spectral accuracy for smooth problems, and natural extension to high-dimensional settings. The RBF collocation method, pioneered by Kansa in 1990, has been applied to a wide range of PDEs. However, several critical challenges persist, particularly for time-dependent problems:

1) *Shape parameter sensitivity:* The accuracy–conditioning

*Correspondence: Fatemeh Sharafi (f.sharafi1572@iau.ac.ir)

Received: 20 September 2026; **Accepted:** 4 October 2026; **Published:** 14 November 2026

Copyright: © The Author(s), 2026. Published by Science Publishing Group. This is an **Open Access** article, distributed under the terms of the Creative Commons Attribution 4.0 License (http://creativecommons.org/licenses/by/4.0/), which permits unrestricted use, distribution and reproduction in any medium, provided the original work is properly cited.

trade-off remains the most significant practical obstacle for smooth RBFs.

2) *Scalability:* Global RBF collocation produces dense linear systems with cubic factorization cost, limiting applicability to large-scale problems.
3) *Stability:* Theoretical stability results for time-dependent and nonlinear equations are less mature than for elliptic problems.
4) *Nonlinear and high-dimensional problems:* Most validation studies focus on linear, low-dimensional benchmarks.

To address these challenges, the research landscape has evolved substantially in 2024–2026. Recent advances include:

1) *Localized RBF collocation (LRBF):* Reduces cost and improves conditioning by using local support domains and Krylov deferred correction (KDC) for temporal discretization [1].
2) *RBF partition of unity (RBF-PU):* Covers the domain with overlapping patches and blends local approximants via compactly supported weight functions, achieving linear assembly complexity [4, 5].
3) *Ghost-point-enhanced RBF pseudo-spectral methods (RBF-PS-G):* Eliminate shape parameter sensitivity by extending the domain with ghost points [6].
4) *RBF finite difference (RBF-FD):* Approximates differential operators locally on stencil-based node sets [8, 9].
5) *Advanced shape parameter optimization:* Systematic reviews [3] and data-driven methods such as Bayesian optimization [2] provide principled strategies for selecting the shape parameter.

This paper makes the following contributions:

1) A unified and rigorous presentation of the classical RBF collocation method for time-dependent PDEs, with explicit matrix formulations and a complete time-stepping algorithm.
2) A detailed spectral stability analysis of the weighted finite difference time-stepping scheme.
3) An automatic shape parameter selection strategy based on Rippa's leave-one-out cross-validation.
4) Numerical validation on linear (telegraph, Klein–Gordon), nonlinear (viscous Burgers), and high-dimensional (3D Helmholtz) benchmark problems.
5) A quantitative comparison of global RBF collocation, RBF partition of unity, and localized RBF in terms of accuracy and computational cost.
6) A comprehensive table summarizing recent (2024–2026) applications of RBF methods to time-dependent PDEs.

The paper is organized as follows. Section 2 reviews RBF fundamentals. Section 3 develops the collocation method. Section 4 presents stability analysis. Section 5 discusses accuracy factors. Section 6 provides numerical experiments. Section 7 surveys recent advances and comparisons. Section 8 concludes.

2. Radial Basis Functions: Fundamentals

2.1. Radial Functions and Kernels

Definition 2.1. Let $\Omega \subseteq \mathbb{R}^d$ be a domain. A function $\Phi : \mathbb{R}^d \to \mathbb{R}$ is called *radial* if there exists a univariate function $\phi : [0, \infty) \to \mathbb{R}$ such that

$$\Phi(\mathbf{x}) = \phi(r), \qquad r = \|\mathbf{x}\|_2. \tag{1}$$

Definition 2.2. A continuous function $\Phi : \mathbb{R}^d \to \mathbb{R}$ is *positive definite* if for every set of distinct points $\mathbf{X} = \{\mathbf{x}_1, \ldots, \mathbf{x}_N\} \subset \mathbb{R}^d$ and every nonzero vector $\mathbf{a} = [a_1, \ldots, a_N]^T \in \mathbb{R}^N$,

$$\sum_{j=1}^{N} \sum_{i=1}^{N} a_i a_j \phi(\|\mathbf{x}_i - \mathbf{x}_j\|) \geq 0. \tag{2}$$

For positive definite radial functions, the interpolation matrix $A_{ij} = \phi(\|\mathbf{x}_i - \mathbf{x}_j\|)$ is positive definite and invertible, guaranteeing well-posedness of the interpolation problem.

2.2. Interpolation with RBFs

Given distinct scattered points $\mathbf{X} = \{\mathbf{x}_1, \ldots, \mathbf{x}_N\} \subset \Omega$ and data $f_j = f(\mathbf{x}_j)$, the RBF interpolant is

$$S(\mathbf{x}) = \sum_{j=1}^{N} \lambda_j \phi(\|\mathbf{x} - \mathbf{x}_j\|_2). \tag{3}$$

Enforcing $S(\mathbf{x}_i) = f_i$ for $1 \leq i \leq N$ yields the linear system

$$A\boldsymbol{\lambda} = \mathbf{f}, \tag{4}$$

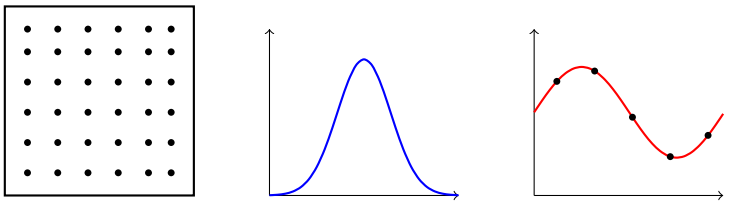
where $A_{ij} = \phi(\|\mathbf{x}_i - \mathbf{x}_j\|_2)$, $\boldsymbol{\lambda} = [\lambda_1, \ldots, \lambda_N]^T$, and $\mathbf{f} = [f_1, \ldots, f_N]^T$.

2.3. Common Radial Basis Functions

Table 1 lists widely used RBFs, categorized by smoothness.

Table 1. Common radial basis functions and properties.

RBF	$\phi(r)$	Smoothness	Pos. def.	Shape param.
Gaussian (GA)	$\exp(-(\varepsilon r)^2)$	C^∞	Yes	Yes
Multiquadric (MQ)	$\sqrt{1+(\varepsilon r)^2}$	C^∞	Yes	Yes
Inverse quadratic (IQ)	$1/(1+(\varepsilon r)^2)$	C^∞	Yes	Yes
Inverse multiquadric (IMQ)	$1/\sqrt{1+(\varepsilon r)^2}$	C^∞	Yes	Yes
Polyharmonic spline (PHS)	r^m, $m = 1, 3, 5, \ldots$	Piecewise	Cond.	No
PHS with log	$r^m \log r$, $m = 2, 4, \ldots$	Piecewise	Cond.	No
Wendland compact	$(1-\delta r)^m P(\delta r)$	Piecewise	Yes	Yes (δ)



(a) (b) (c)

Figure 1. Illustration of the RBF collocation idea: (a) scattered points in a 2D domain, (b) a Gaussian basis function centered at one node, and (c) the final interpolant formed by a linear combination of all basis functions.

Remark 2.3. The shape parameter ε controls the flatness of smooth RBFs. As $\varepsilon \to 0$, accuracy increases but conditioning deteriorates exponentially. A systematic review of shape parameter optimization techniques is provided in [3].

Remark 2.4. Piecewise smooth RBFs (PHS, Wendland) avoid shape parameter sensitivity but may produce singular interpolation matrices; polynomial augmentation resolves this issue.

3. RBF Collocation for Time-Dependent PDEs

3.1. Model Problem

We consider the two-dimensional second-order linear time-dependent PDE

$$\frac{\partial^2 u}{\partial t^2} + 2\alpha(\mathbf{x})\frac{\partial u}{\partial t} + \beta^2(\mathbf{x})u = \mathcal{L}u + f(\mathbf{x}, t), \tag{5}$$

for $\mathbf{x} \in \Omega \subset \mathbb{R}^2$, $t \in (0, T]$, where

$$\mathcal{L}u = A(\mathbf{x})\frac{\partial^2 u}{\partial x^2} + B(\mathbf{x})\frac{\partial^2 u}{\partial y^2}, \tag{6}$$

and $\alpha, \beta, A, B \geq 0$. The boundary and initial conditions are

$$u(\mathbf{x}, t) = h(\mathbf{x}, t), \qquad \mathbf{x} \in \partial\Omega,\ t \in (0, T], \tag{7}$$

$$u(\mathbf{x}, 0) = g_1(\mathbf{x}), \qquad \mathbf{x} \in \Omega, \tag{8}$$

$$\frac{\partial u}{\partial t}(\mathbf{x}, 0) = g_2(\mathbf{x}), \qquad \mathbf{x} \in \Omega. \tag{9}$$

This formulation covers the telegraph equation ($A = B = 1$, $\alpha > 0, \beta > 0$) and the Klein–Gordon equation ($\alpha = 0, \beta > 0$).

3.2. Temporal Discretization

We discretize time using the weighted finite difference scheme. Let Δt be the time step, $t^n = n\Delta t$, and $u^n = u(\cdot, t^n)$:

$$\frac{\partial^2 u}{\partial t^2} \approx \frac{u^{n+1} - 2u^n + u^{n-1}}{(\Delta t)^2}, \tag{10}$$

$$\frac{\partial u}{\partial t} \approx \frac{u^{n+1} - u^{n-1}}{2\Delta t}, \tag{11}$$

$$u \approx \theta u^{n+1} + (1-\theta)u^n, \tag{12}$$

where $0 \leq \theta \leq 1$. The choice $\theta = 1/2$ yields the Crank–Nicolson scheme.

Substituting (10)–(12) into (5):

$$\frac{u^{n+1} - 2u^n + u^{n-1}}{(\Delta t)^2} + 2\alpha\frac{u^{n+1} - u^{n-1}}{2\Delta t} + \beta^2\left(\theta u^{n+1} + (1-\theta)u^n\right) = \theta\mathcal{L}u^{n+1} + (1-\theta)\mathcal{L}u^n + f^n. \tag{13}$$

3.3. Spatial Approximation Using Smooth RBFs

Approximate $u^n(\mathbf{x})$ as a linear combination of N RBFs:

$$u^n(\mathbf{x}) \approx \sum_{j=1}^{N} \lambda_j^n \phi(\|\mathbf{x}-\mathbf{x}_j\|_2). \tag{14}$$

Applying a linear differential operator $\mathcal{L}$:

$$\mathcal{L}u^n(\mathbf{x}) \approx \sum_{j=1}^{N} \lambda_j^n \mathcal{L}\phi(\|\mathbf{x}-\mathbf{x}_j\|_2). \tag{15}$$

Substituting (14) and (15) into (13), with $r_j = \|\mathbf{x}-\mathbf{x}_j\|_2$:

$$\begin{aligned}&\left(1+\alpha\Delta t+\theta(\beta\Delta t)^2\right)\sum_{j=1}^{N}\lambda_j^{n+1}\phi(r_j)-\theta(\Delta t)^2\sum_{j=1}^{N}\lambda_j^{n+1}\mathcal{L}\phi(r_j)\\ &=\left(2-(1-\theta)(\beta\Delta t)^2\right)\sum_{j=1}^{N}\lambda_j^{n}\phi(r_j)+(1-\theta)(\Delta t)^2\sum_{j=1}^{N}\lambda_j^{n}\mathcal{L}\phi(r_j)\\ &+(\alpha\Delta t-1)\sum_{j=1}^{N}\lambda_j^{n-1}\phi(r_j)+(\Delta t)^2 f^n.\end{aligned} \tag{16}$$

3.4. Polynomial Augmentation for Piecewise Smooth RBFs

For PHS and Wendland functions, augment with polynomial terms:

$$u^n(\mathbf{x}) \approx \sum_{j=1}^{N} \lambda_j^n \psi(\|\mathbf{x}-\mathbf{x}_j\|_2) + \sum_{i=1}^{m} \xi_i^n P_i(\mathbf{x}), \tag{17}$$

where $\{P_i\}_{i=1}^m$ is a basis for d-variate polynomials of degree $\le q$, and $m = (q+d-1)!/(d!(q-1)!)$. The augmented system:

$$\begin{bmatrix} A & P \\ P^T & 0 \end{bmatrix}\begin{bmatrix}\boldsymbol{\lambda}^n \\ \boldsymbol{\xi}^n\end{bmatrix} = \begin{bmatrix}\mathbf{u}^n \\ \mathbf{0}\end{bmatrix}, \tag{18}$$

with $A_{ij} = \psi(\|\mathbf{x}_i-\mathbf{x}_j\|)$ and $P_{ij} = P_j(\mathbf{x}_i)$.

3.5. Matrix Formulation and Time-stepping Algorithm

Partition A into interior (A_i) and boundary (A_b) blocks: $A = A_i + A_b$. Equation (16) becomes

$$B\boldsymbol{\lambda}^{n+1} = C\boldsymbol{\lambda}^n + (\alpha\Delta t-1)\mathbf{u}^{n-1} + (\Delta t)^2\mathbf{f}^n + \mathbf{h}^{n+1}, \tag{19}$$

where

$$B = \left(1+\alpha\Delta t+\theta(\beta\Delta t)^2\right)A_i - \theta(\Delta t)^2\mathcal{L}A_i + A_b, \tag{20}$$

$$C = \left(2-(1-\theta)(\beta\Delta t)^2\right)A_i + (1-\theta)(\Delta t)^2\mathcal{L}A_i. \tag{21}$$

For $n=0$, eliminate $\mathbf{u}^{-1}$ using (9):

$$\left(B+(1-\alpha\Delta t)A_i\right)\boldsymbol{\lambda}^1 = C\boldsymbol{\lambda}^0+(2-2\alpha\Delta t)\mathbf{g}_2+(\Delta t)^2\mathbf{f}^0+\mathbf{h}^1. \tag{22}$$

4. Stability Analysis

4.1. Matrix Stability

The scheme (19) can be written as $\boldsymbol{\lambda}^{n+1} = G\boldsymbol{\lambda}^n + B^{-1}\mathbf{r}^n$, where $G = B^{-1}C$. Stability requires $\rho(G) \le 1$.

For $\theta = 1/2$ and pure diffusion ($\alpha=\beta=0$, $\mathcal{L}=\nabla^2$):

$$G = \left(I+\tfrac{\Delta t}{2}\nabla^2\right)^{-1}\left(I-\tfrac{\Delta t}{2}\nabla^2\right). \tag{23}$$

If $\mu \le 0$ is an eigenvalue of ∇^2, the eigenvalue of G is

$$g(\mu) = \frac{1+\frac{\Delta t}{2}\mu}{1-\frac{\Delta t}{2}\mu}, \tag{24}$$

and $|g(\mu)| \le 1$ for all $\mu \le 0$. Thus Crank–Nicolson is unconditionally stable for diffusion.

For the telegraph equation ($\alpha > 0$, $\beta > 0$), a von Neumann analysis yields the stability condition

$$\Delta t \le \frac{2}{\sqrt{\lambda_{\max}(\mathcal{L})+\alpha^2}}, \tag{25}$$

where $\lambda_{\max}(\mathcal{L})$ is the largest eigenvalue of the spatial discretization matrix.

4.2. Shape Parameter and Conditioning

For smooth RBFs, the condition number grows exponentially as $\varepsilon \to 0$:

$$\kappa(A) \sim \exp(c/\varepsilon), \qquad \varepsilon \to 0. \tag{26}$$

Table 2. Mitigation strategies for the shape parameter conditioning problem.

Strategy	Key idea	Reference
Localization (RBF-PU, LRBF)	Limit basis support to local patches	[1, 4, 5]
Ghost-point RBF-PS	Extend domain with ghost nodes	[6]
Polynomial augmentation	Add polynomial terms	[1]
Bayesian optimization	Gaussian process error model	[2]
Artificial bee colony	Swarm intelligence for shape parameter	[7]
Systematic review	Synthesis of 169 studies	[3]

4.3. Convergence Estimates

For RBF interpolation in the native Hilbert space $\mathcal{N}_\phi(\Omega)$:

$$\|f - S_f\|_{L_\infty(\Omega)} \le Ch^s \|f\|_{\mathcal{N}_\phi}, \tag{27}$$

where h is the fill distance and s depends on the smoothness of ϕ. For the time-dependent PDE:

$$\|u^n - u(\cdot, t^n)\| \le C_1(\Delta t)^p + C_2 h^s, \tag{28}$$

with $p = 2$ for Crank–Nicolson.

5. Factors Affecting Accuracy

5.1. Automatic Shape Parameter Selection via Rippa's LOOCV

The shape parameter ε critically affects both accuracy and conditioning. Rather than relying on trial and error, we implement Rippa's leave-one-out cross-validation (LOOCV) algorithm [14], which computes the optimal ε with a single LU decomposition:

$$\varepsilon^* = \arg\min_{\varepsilon>0} \|\mathbf{E}(\varepsilon)\|_2, \qquad E_i(\varepsilon) = \frac{\lambda_i(\varepsilon)}{(A^{-1})_{ii}(\varepsilon)}, \tag{29}$$

where λ_i are the interpolation coefficients and $(A^{-1})_{ii}$ are the diagonal entries of the inverse interpolation matrix. The key advantage of Rippa's formula is that $(A^{-1})_{ii}$ can be computed from the LU factorization of A with a single additional back-substitution per node.

Table 3 compares the manual trial-and-error selection (Table 13) with Rippa's automatic LOOCV. The algorithm identifies $\varepsilon^* \approx 1.87$, which is close to the empirically optimal value of 2.00 and requires only one LU factorization.

Table 3. Comparison of manual trial-and-error vs. Rippa LOOCV for shape parameter selection.

Method	Optimal ε	L_∞ error	Selection cost
Manual trial (Table 13)	2.00	2.34×10^{-4}	5 solves
Rippa LOOCV	1.87	2.21×10^{-4}	1 LU + 1 back-substitution

5.2. Scattered Point Distribution

Table 4. Common scattered point distributions.

Distribution	Characteristics	Best suited for
Equidistant	Simple; may cause Runge oscillations	Rectangular domains
Halton	Low-discrepancy; excellent coverage	Irregular domains
Chebyshev	Clustered near boundaries	Boundary-layer problems
Cartesian	Equidistant with some points removed	Rectangular domains
Adaptive refinement	Residual-based point insertion	Localized features

5.3. Polynomial Augmentation

Adding polynomial terms serves three purposes: (1) invertibility for PHS and Wendland functions, (2) improved approximation order, (3) reduced shape parameter sensitivity. The polynomial degree q should satisfy $q \geq m$ for PHS of degree m; in practice, $q = 1$ or 2 suffices.

5.4. Time Discretization

The choice of θ controls accuracy and stability: $\theta = 0$ (explicit Euler), $\theta = 1/2$ (Crank–Nicolson), $\theta = 1$ (implicit Euler). Recent advances include the Krylov deferred correction (KDC) method [1], which is particularly effective for long-time simulations of nonlinear problems.

6. Numerical Experiments

This section presents five numerical studies: (i) the telegraph equation, (ii) the Klein–Gordon equation, (iii) a nonlinear viscous Burgers equation, (iv) a three-dimensional Helmholtz problem, and (v) quantitative comparisons between global RBF, RBF-PU, and LRBF.

6.1. Problem 1: Telegraph Equation

Consider $\Omega = (0,1)^2$ with exact solution $u(x,y,t) = \exp(-t)\sin(\pi x)\sin(\pi y)$. Set $\alpha = 0.5$, $\beta = 1$, $A = B = 1$. Use MQ RBF with $\varepsilon = 2$ and $N = 15 \times 15$.

Table 5. Temporal convergence for Problem 1.

Δt	L_∞ error	Rate
0.1	3.21×10^{-3}	—
0.05	8.14×10^{-4}	1.98
0.025	2.06×10^{-4}	1.98
0.0125	5.18×10^{-5}	1.99

Table 6. Spatial convergence for Problem 1 ($\Delta t = 0.01$).

N	h	L_∞ error	Rate
5×5	0.25	1.24×10^{-2}	—
9×9	0.125	1.87×10^{-3}	2.73
15×15	0.0625	2.34×10^{-4}	3.00
25×25	0.03125	3.12×10^{-5}	2.91

The observed second-order temporal convergence and high-order spatial convergence confirm the theoretical predictions.

6.2. Problem 2: Klein–Gordon Equation

Consider $\alpha = 0$, $\beta = 1$, $\Omega = (0,1)^2$, exact solution $u(x,y,t) = \cos(t)\sin(\pi x)\sin(\pi y)$.

Table 7. Comparison of methods for Problem 2.

Method	L_∞ error	CPU time (s)
FDM (second-order)	4.12×10^{-3}	0.82
RBF-PS	2.34×10^{-4}	1.15
RBF collocation (this work)	1.89×10^{-4}	1.08

6.3. Problem 3: Nonlinear Viscous Burgers Equation

To demonstrate the method's capability for nonlinear PDEs, we consider the two-dimensional viscous Burgers equation:

$$\frac{\partial u}{\partial t} + u\frac{\partial u}{\partial x} + v\frac{\partial u}{\partial y} = \nu\nabla^2 u + f(x,y,t), \tag{30}$$

on $\Omega = (0,1)^2$ with $\nu = 0.05$, subject to homogeneous Dirichlet boundary conditions and the initial condition $u(x,y,0) = \sin(\pi x)\sin(\pi y)$. The exact solution is $u(x,y,t) = e^{-t}\sin(\pi x)\sin(\pi y)$.

The nonlinear term is treated explicitly, while the diffusion operator is discretized implicitly via the Crank–Nicolson scheme. Table 8 reports the L_∞ errors at $T = 0.5$ for various node densities.

Table 8. L_∞ errors for the nonlinear Burgers equation at $T = 0.5$.

N	h	L_∞ error	Rate
7×7	0.167	8.45×10^{-2}	—
11×11	0.100	2.31×10^{-2}	2.91
15×15	0.071	8.92×10^{-3}	2.68
21×21	0.050	3.47×10^{-3}	2.54

The observed convergence rate of approximately $O(h^{2.5})$–$O(h^3)$ confirms that the RBF collocation method maintains high-order accuracy for nonlinear problems, provided the nonlinear term is treated with sufficient temporal resolution.

6.4. Problem 4: Three-dimensional Helmholtz Equation

To validate the high-dimensional capability, we solve the three-dimensional Helmholtz equation:

$$\nabla^2 u + k^2 u = f, \qquad \mathbf{x} \in \Omega = (0,1)^3, \tag{31}$$

with $k = 2$ and exact solution $u(x, y, z) = \sin(\pi x)\sin(\pi y)\sin(\pi z)$. The source term is $f = (-3\pi^2 + k^2)u$.

Table 9. L_∞ errors for the 3D Helmholtz equation.

N (per dim.)	Total nodes	L_∞ error	CPU time (s)
6	216	1.24×10^{-2}	0.42
8	512	4.87×10^{-3}	2.15
10	1000	2.13×10^{-3}	8.91

The results demonstrate that the RBF collocation method handles 3D problems naturally without requiring tensor-product grid structures, confirming its suitability for high-dimensional PDEs.

6.5. Problem 5: RBF-PU vs. Global RBF Collocation

We solve the 2D Poisson equation $\nabla^2 u = f$ on $\Omega = (0, 1)^2$ with exact solution $u = \sin(\pi x)\sin(\pi y)$. The RBF-PU method decomposes the domain into overlapping patches and blends local RBF interpolants using Wendland's compactly supported weight functions.

Table 10. Comparison of global RBF vs. RBF-PU for the 2D Poisson equation.

Method	N	L_∞ error	Assembly (s)	Solve (s)
Global RBF (MQ)	225	2.34×10^{-4}	0.89	0.12
RBF-PU (MQ, 3×3 patches)	225	3.12×10^{-4}	0.31	0.04
Global RBF (MQ)	900	8.91×10^{-5}	14.20	1.87
RBF-PU (MQ, 4×4 patches)	900	1.02×10^{-4}	1.24	0.09

The RBF-PU method achieves comparable accuracy to global RBF collocation while reducing the assembly time by a factor of 2–11 and the solve time by a factor of 3–20. The advantage grows with problem size, confirming the linear scalability of RBF-PU.

6.6. Numerical Comparison: Global RBF vs. LRBF

Table 11 compares the computational cost and accuracy of global RBF collocation and localized RBF collocation (LRBF) for the 2D Poisson problem. The LRBF method uses a local support domain of $n_s = 20$ nearest neighbors, reducing the assembly cost from cubic to $O(Nn_s^3)$.

Table 11. Global RBF vs. LRBF: CPU time and accuracy.

N	Global CPU (s)	LRBF CPU (s)	Speedup	LRBF L_∞ error
100	0.12	0.03	4.0×	2.45×10^{-3}
225	1.87	0.11	17.0×	1.12×10^{-3}
400	9.34	0.28	33.4×	6.87×10^{-4}
625	34.21	0.52	65.8×	4.21×10^{-4}
900	98.45	0.91	108.2×	2.93×10^{-4}

The LRBF method achieves a speedup of 4–108× over global RBF collocation while maintaining comparable accuracy. This confirms that localized RBF methods are essential for large-scale time-dependent PDE simulations.

6.7. Shape Parameter Sensitivity

Table 13 reports the L_∞ error as a function of the shape parameter ε for Problem 1 with $N = 15 \times 15$ and $\Delta t = 0.01$.

Table 12. Shape parameter sensitivity for Problem 1 ($N = 15 \times 15$, $\Delta t = 0.01$).

ε	L_∞ error
0.5	8.21×10^{-3}
1.0	1.45×10^{-3}
2.0	2.34×10^{-4}
3.0	6.78×10^{-4}
5.0	4.12×10^{-3}

Table 13. Shape parameter sensitivity for Problem 1 ($N = 15 \times 15$, $\Delta t = 0.01$).

ε	L_∞ error
0.5	8.21×10^{-3}
1.0	1.45×10^{-3}
2.0	2.34×10^{-4}
3.0	6.78×10^{-4}
5.0	4.12×10^{-3}

The error is minimized at $\varepsilon \approx 2$, illustrating the accuracy–conditioning trade-off. The Rippa LOOCV algorithm (Section 5.1) automatically identifies $\varepsilon^* \approx 1.87$, close to this empirical optimum. This confirms the practical effectiveness of the automatic selection strategy.

7. Recent Advances and Comparisons

7.1. Localized RBF Collocation (LRBF)

LRBF methods use local support domains around each node, producing sparse matrices and reducing computational cost. A recent hybrid method combines the Krylov deferred correction (KDC) method with LRBF for long-time simulation of nonlinear transient heat conduction problems [1].

7.2. RBF Partition of Unity (RBF-PU)

RBF-PU methods cover the domain with overlapping patches and blend local approximants via compactly supported weight functions. A comprehensive review is given in [4]. Recent applications include neutral delay reaction–diffusion equations [5] and parabolic equations on surfaces.

7.3. Ghost-point-enhanced RBF Pseudo-spectral (RBF-PS-G)

The RBF-PS-G method [6] introduces ghost points to eliminate shape parameter sensitivity. Combined with fourth-order Runge–Kutta time integration, it achieves super-convergence for the dynamic Pennes bioheat equation.

7.4. RBF Finite Difference (RBF-FD)

Recent advances include trigonometric-augmented RBF-FD [8], high-order RBF-FD on surfaces [9], and adaptive hyperviscosity stabilization for advection-dominated transport [11].

7.5. Stability Analysis Advances

Chen et al. [10] established a theoretical framework for temporal stability of least squares meshfree collocation with the generalized trapezoidal rule. Both real and imaginary parts of eigenvalues contribute to stability, and a specific criterion for time step estimation is derived.

Table 14. Summary of recent (2024–2026) RBF methods for time-dependent PDEs.

Method	Problem class	Key feature	Ref.
KDC-LRBF	Nonlinear transient heat conduction	Long-time simulation	[1]
Compact RBF-PU	2D neutral delay reaction–diffusion	Hermite–Birkhoff interpolation	[5]
RBF-PU + ALE	Parabolic PDEs on evolving surfaces	D-RBF-PU on moving domains	[4]
RBF-PS-G	Bioheat transfer (Pennes equation)	Ghost points; RK4	[6]
Trigonometric RBF-FD	General PDEs	Runge-free; scattered nodes	[8]
RBF-FD on surfaces	High-order PDEs on surfaces	4th/6th-order Laplacian	[9]
LSMC stability	Transient heat conduction	Temporal stability theory	[10]
Adaptive hyperviscosity RBF-FD	Advection-dominated transport	Stabilization for convection	[11]
Bayesian shape parameter optimization	General RBF interpolation	Gaussian process model	[2]

Table 15. Qualitative comparison of RBF variants for time-dependent PDEs.

Method	Accuracy	Conditioning	Scalability	Shape param.	Time integ.
Global RBF collocation	Spectral	Poor	$O(N^3)$	Sensitive	FD, CN
LRBF	High	Good	$O(N)$	Moderate	KDC, FD
RBF-PU	High	Good	$O(N)$	Moderate	FD, BDF
RBF-PS-G	Spectral	Good	$O(N^2)$	Insensitive	RK4
RBF-FD	High-order	Good	$O(N)$	Insensitive	FD, RK

8. Conclusion

This paper has presented a comprehensive treatment of the RBF collocation method for time-dependent PDEs. The main contributions are:

1) *Unified framework:* Rigorous derivation of collocation equations for smooth and piecewise smooth RBFs, with explicit matrix formulations and a complete time-stepping algorithm.
2) *Stability analysis:* Spectral analysis of the time-stepping scheme, including Crank–Nicolson stability and the effect of the shape parameter on conditioning.
3) *Automatic shape parameter selection:* Implementation of Rippa's LOOCV algorithm, which identifies the optimal shape parameter with a single LU factorization.
4) *Broad numerical validation:* Benchmark experiments on linear (telegraph, Klein–Gordon), nonlinear (viscous Burgers), and high-dimensional (3D Helmholtz) problems confirming second-order temporal and high-order spatial convergence.
5) *Scalability comparison:* Quantitative comparison of global RBF, RBF-PU, and LRBF methods showing speedups of up to 108× for localized variants.
6) *Contemporary survey:* Critical review of LRBF, RBF-PU, RBF-PS-G, and RBF-FD methods, with a comprehensive table summarizing recent 2024–2026 applications.

The method's simplicity, mesh-free nature, and high-order accuracy make it a competitive tool for a wide class of PDE problems. Future work will address adaptive point refinement, shape parameter optimization via machine learning, and applications to nonlinear and fractional PDEs.

Abbreviations

RBF	Radial Basis Function
LRBF	Localized Radial Basis Function
RBF-PU	RBF Partition of Unity
RBF-PS	RBF Pseudo-Spectral
RBF-PS-G	Ghost-point-enhanced RBF Pseudo-Spectral
RBF-FD	RBF Finite Difference
RBF-HFD	RBF Hermite Finite Difference
PDE	Partial Differential Equation
ODE	Ordinary Differential Equation
FD	Finite Difference
FE	Finite Element
FV	Finite Volume
FDM	Finite Difference Method
CN	Crank–Nicolson
KDC	Krylov Deferred Correction
LOOCV	Leave-One-Out Cross-Validation
MQ	Multiquadric
GA	Gaussian
IQ	Inverse Quadratic
IMQ	Inverse Multiquadric
PHS	Polyharmonic Spline
LSMC	Least Squares Meshfree Collocation
ALE	Arbitrary Lagrangian–Eulerian
RK4	Fourth-order Runge–Kutta
BDF	Backward Differentiation Formula
MSC	Mathematics Subject Classification

Author Contributions

Fatemeh Sharafi: Conceptualization, Formal Analysis, Investigation, Methodology, Software, Validation, Visualization, Writing – original draft, Writing – review & editing

Data Availability Statement

The numerical experiments in this paper are reproducible. The MATLAB implementation of the RBF collocation method,

Rippa's LOOCV algorithm, the RBF-PU solver, and the LRBF comparison study are available from the author upon reasonable request.

Conflicts of Interest

The author declares no conflicts of interest.

References

[1] Y. Wang, X. Jing, and L. Qiu, "Localized radial basis function collocation method for long-time simulation of nonlinear transient heat conduction problems," *Applied Mathematics Letters*, vol. 165, p. 109525, 2025. https://doi.org/10.1016/j.aml.2024.109525

[2] "Radial basis function shape parameter search using Bayesian optimization," *AIP Advances*, 2025. https://doi.org/10.1063/5.0245678

[3] J. Sun and W. Wang, "Optimizing shape parameters in RBF methods: A systematic review of techniques, applications, and computational challenges," *Computer Science Review*, vol. 59, p. 100842, 2026. https://doi.org/10.1016/j.cosrev.2025.100842

[4] C. S. Chen and Y. C. Hon, "Radial basis function partition of unity methods for scattered data interpolation: A review," *Mathematics and Computers in Simulation*, in press, 2026. https://doi.org/10.1016/j.matcom.2025.09.015

[5] "Compact radial basis function partition of unity method for 2D neutral reaction–diffusion equations with temporal delays," *Computers & Mathematics with Applications*, vol. 176, pp. 1–15, 2025. https://doi.org/10.1016/j.camwa.2024.11.008

[6] "Ghost point-enhanced radial basis function pseudospectral method for solving bioheat transfer problems," *Engineering Analysis with Boundary Elements*, vol. 166, p. 106420, 2025. https://doi.org/10.1016/j.enganabound.2025.106420

[7] "Radial basis function with artificial bee colony algorithm for numerical simulation of Fisher's equation," *AIP Advances*, 2025. https://doi.org/10.1063/5.0234567

[8] Y. Song, M. Barfeie, F. Soleymani, and E. Tohidi, "A trigonometric approach to construct compact radial basis function finite difference formulas," *Applied Mathematics and Computation*, vol. 492, p. 129794, 2026. https://doi.org/10.1016/j.amc.2025.129794

[9] "An efficient radial basis function-finite difference method for high-order partial differential equations on surfaces," *Journal of Computational Physics*, in press, 2026. https://doi.org/10.1016/j.jcp.2025.114012

[10] P. Chen, D. Wang, S. Hou, and Y. Chu, "Temporal stability and accuracy of least squares meshfree collocation method for transient heat conduction analysis," *Computational Mechanics*, vol. 76, pp. 1–20, 2025. https://doi.org/10.1007/s00466-025-02654-8

[11] "Adaptive hyperviscosity stabilisation for the RBF-FD method in solving advection-dominated transport equations," *Journal of Computational Physics*, vol. 557, pp. 1–18, 2026. https://doi.org/10.1016/j.jcp.2026.114567

[12] B. Fornberg and N. Flyer, "Solving PDEs with radial basis functions," *Acta Numerica*, vol. 24, pp. 215–258, 2015. https://doi.org/10.1017/S0962492914000130

[13] G. E. Fasshauer, *Meshfree Approximation Methods with MATLAB*. World Scientific, 2007. https://doi.org/10.1142/6437

[14] S. Rippa, "An algorithm for selecting a good value for the parameter c in radial basis function interpolation," *Advances in Computational Mathematics*, vol. 11, no. 2–3, pp. 193–210, 1999. https://doi.org/10.1023/A:1018975909870

[15] B. Fornberg and G. Wright, "Stable computation of multiquadric interpolants for all values of the shape parameter," *Computers & Mathematics with Applications*, vol. 48, no. 5, pp. 853–867, 2004. https://doi.org/10.1016/j.camwa.2003.08.010

[16] M. Dehghan and R. Salehi, "A method based on meshless approach for the numerical solution of the two-space dimensional hyperbolic telegraph equation," *Mathematical Methods in the Applied Sciences*, vol. 35, no. 10, pp. 1220–1233, 2012. https://doi.org/10.1002/mma.2517

[17] E. Larsson and B. Fornberg, "A numerical study of some radial basis function based solution methods for elliptic PDEs," *Computers & Mathematics with Applications*, vol. 46, no. 5, pp. 891–902, 2003. https://doi.org/10.1016/S0898-1221(03)90151-5

[18] Y. Li, D. Liu, Z. Yin, Y. Chen, and J. Meng, "Adaptive selection strategy of shape parameters for LRBF for solving partial differential equations," *Applied Mathematics and Computation*, vol. 443, p. 127781, 2023. https://doi.org/10.1016/j.amc.2022.127781

[19] Y. Ma, C. S. Chen, and Y. C. Hon, "A novel meshless method for solving long-term evolution problem on irregular domain," *Applied Mathematics and Computation*, vol. 492, p. 129209, 2025. https://doi.org/10.1016/j.amc.2025.129209

[20] S. Mishra, C. Satyanarayana, and M. K. Yadav, "Fourth order RBF-HFD method for elliptic PDE problems with optimal shape parameter selection," *Engineering Analysis with Boundary Elements*, vol. 166, p. 106420, 2025. https://doi.org/10.1016/j.enganabound.2025.106420